Progress on Structural Analysis of Advanced Materials

Progress on Structural Analysis of Advanced Materials

Edited by

George C. Papanicolaou and
Dionysis E. Mouzakis

Cambridge
Scholars
Publishing

Progress on Structural Analysis of Advanced Materials

Edited by George C. Papanicolaou and Dionysis E. Mouzakis

This book first published 2026

Cambridge Scholars Publishing

Lady Stephenson Library, Newcastle upon Tyne, NE6 2PA, UK

British Library Cataloguing in Publication Data
A catalogue record for this book is available from the British Library

ISBN: 978-1-0364-6996-2
ISBN (Ebook): 978-1-0364-6997-9

TABLE OF CONTENTS

CHAPTER 1

ON THE DECOUPLING OF FRACTURE MODES IN INTERLAMINAR FRACTURE TESTS ON BI-MATERIAL SPECIMENS

P. TSOKANAS[1], L.F.M. DA SILVA[2], F. MUJIKA[3], A. ARRESE[3], P. FISICARO[4] AND P.S. VALVO[4]

[1]INEGI, 4200-465 PORTO, PORTUGAL

[2]FACULDADE DE ENGENHARIA, UNIVERSIDADE DO PORTO, 4200-465 PORTO, PORTUGAL

[3]FACULTY OF ENGINEERING OF GIPUZKOA, UNIVERSITY OF THE BASQUE COUNTRY, 20018 SAN SEBASTIÁN, SPAIN

[4]DEPARTMENT OF CIVIL AND INDUSTRIAL ENGINEERING, UNIVERSITY OF PISA, IT-56122 PISA, ITALY

Abstract

We start by reviewing methods for fracture mode decoupling in unconventional laboratory specimens. Then, we propose energetically orthogonal mode decoupling conditions and associated specimen design criteria to obtain pure fracture modes when bi-material specimens are tested in asymmetric double cantilever beam and asymmetric end-notched flexure test configurations. This work hopefully sheds light on some controversial points in the relevant literature.

Introduction

We consider laboratory tests for measuring the interlaminar fracture toughness of a delamination specimen. Such tests can generally be modelled by considering the specimen as a plane (two-dimensional) cracked body, while the crack propagates in a mix of the basic fracture modes I (opening) and II (sliding). If this body is symmetrically cracked (Fig. 1.1.a), fracture modes I and II are respectively associated to systems of symmetric and antisymmetric forces with respect to the crack plane. These forces respectively produce only normal stresses, σ_n (or crack-tip normal forces, F_n), and transverse relative displacements, δ_n, or only shear stresses, σ_t (or crack-tip shear forces, F_t), and axial relative displacements, δ_t, on the crack plane around the crack tip (Fig. 1.1.b). These simple pure-mode conditions do not apply in general for asymmetrically cracked bodies (Fig. 1.1.c), such as bi-material specimens.

In this presentation, we will revisit the problem of fracture mode decoupling and again propose pure-mode conditions and derive associated specimen design criteria, aiming to resolve the controversial points in the literature. We focus on the asymmetric double cantilever beam (ADCB) (Fig. 1.1.d) and asymmetric end-notched flexure (AENF) (Fig. 1.1.e) test configurations, also assuming that both sub-beams are homogeneous and special orthotropic. This work assumes that pure mode I conditions occur when $\delta_t = 0$. Then, by enforcing energetical orthogonality with mode II, it follows that pure mode II conditions occur when $F_n = 0$. Using these pure-mode conditions, and by developing a simple mechanical model using laminated beam theory, Engesser–Castigliano's theorem, and unit-load method —this work was very recently published in (Mujika et al. 2023, 109454), we derive the specimen design criteria for bi-material specimens loaded using the ADCB and AENF test configurations from scratch. We will show that the two criteria to obtain pure mode I in the ADCB test and pure mode II in the AENF test coincide and are aligned with the criterion used in part of the existing literature. We hope that the present work helps resolve the confusion in the literature regarding the correctness of different mode decoupling conditions.

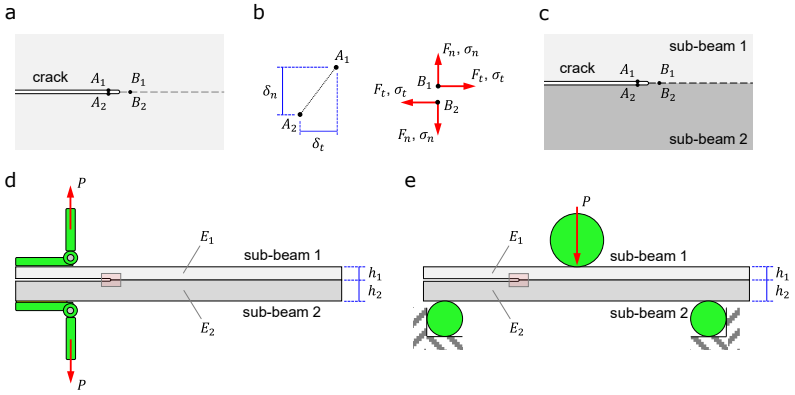

Fig. 1-1 (a) Symmetric crack problem; (b) relative displacements, forces, and stresses near the crack tip; (c) asymmetric crack problem; and (d) ADCB and (e) AENF test configurations.

Existing Pure-Mode Conditions and Specimen Design Criteria

Energetically orthogonal pure-mode conditions

Valvo (2012, 1-20) demonstrated that the 'standard' virtual crack closure technique (VCCT)—based on the decomposition of the crack-tip nodal forces into symmetric and antisymmetric components—may be inappropriate when analysing problems with highly asymmetric cracks since negative values may be calculated for either mode I, G_I, or mode II, G_{II}, contributions to the energy release rate (ERR), G. To remedy this shortcoming, the author suggested defining pure modes based on energetically orthogonal systems of forces at the crack tip. In this way, always non-negative modal contributions to the ERR are obtained. At first, he proposed to identify pure mode I as the case when $F_t = 0$, and pure mode II as the case when $\delta_n = 0$. In a subsequent work (Valvo 2015, 235-244), the same author reconsidered his proposal and suggested the following conditions instead: pure mode I occurs when $\delta_t = 0$, and pure mode II occurs when $F_n = 0$. The more recent proposal has a more convincing physical basis, as it assumes that mode I fracture corresponds to a pure opening of the crack faces.

Similarly to Valvo, Harvey and Wang (2012, 329-352; Harvey and Wang 2012, 737-759) developed an orthogonal pure mode methodology

for partitioning the ERR into its modal contributions. They assumed that the mode I loading condition must be orthogonal to the mode II loading condition through the ERR 'space'. Using this, any pure-mode condition can be identified experimentally, theoretically, or numerically, and the orthogonality condition can then be used to find the other pure modes. The authors defined two sets of pure-mode conditions:

- Set 1: Pure mode I exists when $\delta_t = 0$, and pure mode II exists when $F_n = 0$
- Set 2: Pure mode I exists when $F_t = 0$, and pure mode II exists when $\delta_n = 0$

Interestingly, their first and second sets of pure modes respectively correspond to the two pure-mode sets proposed by Valvo in (Valvo 2015, 235-244; Valvo 2012, 1-20). Harvey and Wang derived the pure modes in the contexts of Euler and Timoshenko beam theories for *rigid* interfaces and the ADCB configuration. Euler beam theory can predict negative G_I/G or G_{II}/G components over a certain number of loading conditions. Although Valvo (Valvo 2012, 1-20) and other authors (Maimí et al. 2018, 36-46) state that this lacks physical interpretation, Harvey and Wang argue that there is no physical requirement on the modal contributions to the ERR, G_I and G_{II}, and the only physical requirement is that G must be non-negative definite since creating new crack surfaces requires energy.

Specimen design criteria

We now focus on the ADCB test configuration, considering both material and geometric asymmetry (Fig. 1.1.d), as the specimen consists of two sub-beams of different longitudinal Young's moduli, E_i, and thicknesses, h_i, $i \in \{1, 2\}$. A reasonable question is whether we can appropriately design the specimen (e.g. define Young's moduli and thicknesses of both sub-beams) to achieve pure-mode I conditions (at the crack tip). Two mode decoupling conditions can be recognised in the literature:

Mode decoupling is achieved when the differential equation of the mode I fracture is only governed by σ_n and δ_n (e.g. Ouyang, Ji, and Li 2011, 031020)

Mode decoupling is achieved when the bending rigidities of the two sub-beams are equal (e.g. Jiang, Wan, and Wu 2016, 374-385)

These conditions lead to the following specimen design criteria:

$$E_1 h_1^2 = E_2 h_2^2 \quad \text{and} \quad E_1 h_1^3 = E_2 h_2^3,$$

Although both are used in literature, both cannot be correct. Thus, our work aims to elucidate which one is ultimately correct.

The Proposed Specimen Design Criteria

In this presentation, we will revisit the problem of fracture mode decoupling and discuss the various proposed definitions for pure-mode conditions, aiming to clarify which theoretical definitions for pure modes are to be preferred. We will focus on the ADCB and AENF test configurations, assuming that both sub-beams are homogeneous and special orthotropic. The work assumes that under pure mode I conditions, $\delta_t = 0$, while under pure mode II conditions, $F_n = 0$ (Valvo 2015, 235-244; Wang and Harvey 2012, 329-352; Harvey and Wang 2012, 737-759). Using this set of conditions and by developing a mechanical model employing laminated beam theory, Engesser–Castigliano's theorem, and unit-load method (Mujika et al. 2023, 109454), we will derive the mode decoupling conditions for bi-material specimens loaded using the ADCB and AENF test configurations from scratch. We will show that the two conditions to obtain pure mode I in the ADCB test and pure mode II in the AENF test coincide and are the same with the first equation of Eqs. (1) that is being used in part of the literature (e.g. Ouyang, Ji, and Li 2011, 031020). In addition, we will demonstrate that the analysis of the AENF test may get complicated by the contact phenomena occurring between the two sub-beams. This contact may alter the general rules for fracture mode partitioning (Dadej et al. in preparation).

We hope that the present work sheds light on the confusion in the literature regarding the correctness of different mode decoupling conditions and associated specimen design formulae. More details and insights may be found in (Mujika et al. 2023, 109454; Dadej et al. in preparation). The present work can be extended by deriving specimen design criteria for multidirectional laminated specimens (Garulli et al. 2020, 773-790).

Acknowledgements

PT and LFMdS acknowledge the financial support of FCT through the PTDC/EME-EME/6442/2020 project. FM and AA acknowledge the financial support of UPV/EHU to the GIU20/060 research group.

References

Dadej, Krzysztof; Bieniaś, Jarosław; Fisicaro, Paolo; Valvo, Paolo S. (in preparation). "*S.*" *Engineering Fracture Mechanics* (in preparation).

Garulli, Tommaso; Catapano, Alfonso; Fanteria, Daniele; Jumel, Julien; Martin, Eric. 2020. "Design and Finite Element Assessment of Fully Uncoupled Multi-Directional Layups for Delamination Tests". *Journal of Composite Materials*, 54(6): 773–790.

Harvey, Christopher M.; Wang, Shu. 2012. "Mixed-Mode Partition Theories for One-Dimensional Delamination in Laminated Composite Beams". *Engineering Fracture Mechanics*, 96: 737–759.

Jiang, Zhiqiang; Wan, Shouhong; Wu, Zhi. 2016. "Calculation of Energy Release Rate for Adhesive Composite/Metal Joints under Mode-I Loading Considering Effect of the Non-Uniformity". *Composites Part B: Engineering*, 95: 374–385.

Maimí, Pere; Gascons, Noemí; Ripoll, Laura; Llobet, Jordi. 2018. "Mixed Mode Delamination of Asymmetric Beam-Like Geometries with Cohesive Stresses". *International Journal of Solids and Structures*, 155: 36–46.

Mujika, Fermin; Tsokanas, Paris; Arrese, Alfredo; Valvo, Paolo S.; da Silva, Lucas F. M. 2023. "Mode Decoupling in Interlaminar Fracture Toughness Tests on Bi-material Specimens". *Engineering Fracture Mechanics*, 290: 109454.

Ouyang, Zheng; Ji, Guangbin; Li, Guangyu. 2011. "On Approximately Realizing and Characterizing Pure Mode-I Interface Fracture Between Bonded Dissimilar Materials". *Journal of Applied Mechanics*, 78(3): 031020.

Valvo, Paolo S. 2012. "A Revised Virtual Crack Closure Technique for Physically Consistent Fracture Mode Partitioning". *International Journal of Fracture*, 173: 1–20.

Valvo, Paolo S. 2015. "A Further Step Towards a Physically Consistent Virtual Crack Closure Technique". *International Journal of Fracture*, 192: 235–244.

Wang, Shu; Harvey, Christopher M. 2012. "Mixed Mode Partition Theories for One Dimensional Fracture". *Engineering Fracture Mechanics*, 79: 329–352.

CHAPTER 2

DETECTABILITY OF NOTCHES IN PLATES USING MULTI-MODAL LAMB WAVES

A.D. GRIGUȚA[1], M.V. PREDOI [2] AND C.C. PETRE[3]

[1]DEPARTMENT OF MECHANICS, UNIVERSITY POLITEHNICA OF BUCHAREST, SPLAIUL INDEPENDENȚEI, 313, 060042, BUCHAREST, ROMANIA

[2]DEPARTMENT OF MECHANICS, UNIVERSITY POLITEHNICA OF BUCHAREST, SPLAIUL INDEPENDENȚEI, 313, 060042, BUCHAREST, ROMANIA

[3]DEPARTMENT OF STRENGTH OF MATERIALS, UNIVERSITY POLITEHNICA OF BUCHAREST, SPLAIUL INDEPENDENȚEI, 313, 060042, BUCHAREST, ROMANIA

Abstract

Notches in plates can be detected using classical nondestructive testing, with ultrasonic waves sent perpendicular to the surface. However, considering the long-range propagation of the Lamb waves, inspection can be made by sending the ultrasonic waves along the plate. There are many prior investigations which state the above idea. In this paper, the interest is to correlate the central frequency of the transducer in use, with the capacity to detect different sizes of notches. The choice of adequate parameters has been done by developing finite elements simulations in COMSOL (COMSOL AB 2023), on a specific plate. The results show that the manufactured notch is detected at every frequency in the proposed range (1 - 2MHz). Nonetheless, it is important to determine graphics in which are shown the propagative modes with high accuracy.

Introduction

Ultrasonic testing is a principal technique in non-destructive testing, being applied in the majority of industrial branches. The use of this technique is an important step ahead in aerospace structure testing for fatigue cracks/notches detection. This technique is used in a wide range of testing parts in different other domains.

Prior studies have shown that the classic technique in which the wave is applied perpendicular to the surface of the structure provides good results. However, the application of this specific technique for a wide structure is time consuming. The guided waves technique has been developed by using ultrasonic waves applied directly along the thin layer of the planar structure. Nonetheless by applying the waves in this manner, the inspection covers a long distance, but the theoretical aspects and the raw data analysis are more complex for these guided Lamb waves. Papers and books regarding the guided wave theory (Achenbach 1973; Graff 1975), numerical simulations (Predoi and Petre 2003, 150; Predoi, Griguța, and Petre 2022) and experiments have been proposed mostly for the propagation of Lamb waves (Griguța and Predoi 2021) and some had studied the edge reflection (Predoi and Rousseau 2003) and detection of defects too, e.g. (Grondel et al. 2003, 137-146).

This paper focuses on the correlation between the dimension of the surface defects and their possible detection, using different central frequencies of the longitudinal waves transducer, which sends several Lamb modes simultaneously. The results are obtained using COMSOL Multiphysics Finite Element Method (FEM) simulations. The obtained results provide a graphic visualization as the Position-Time plots of the FEM results, which are then post-processed in MATLAB (The MathWorks, Inc. 2017).

The proposed simulation is according to the geometry and material of a specific plate. Different applications were proposed for each of the considered frequencies in order to have both, the correlation between the maximal size of the finite element and the frequency and the favorable graphic time dependent transducer pulse impulse (mathematical expression regarding the Gaussian envelope).

In order to present these results, it is important to understand the concept of ultrasonic Lamb waves. Therefore, theoretical knowledge is mandatory to be understood with the multimode propagation concept presented in more details in (Griguța and Predoi 2021). In the case of Lamb waves two different modes of propagation appear, symmetrical and asymmetrical. The expression of displacements for each case are as follows:

Symmetrical:

$$u = [iS_L k_x \cos(k_{Lz} z) - S_T k_{Tz} \cos(k_{Tz} z)] e^{i(k_x x - \omega t)}$$

$$w = [-S_L k_{Lz} \sin(k_{Lz} z) + iS_T k_x \sin(k_{Tz} z)] e^{i(k_x x - \omega t)} \quad (1)$$

Asymmetrical:

$$u = [iA_L k_x \cos(k_{Lz} z) + A_T k_{Tz} \cos(k_{Tz} z)] e^{i(k_x x - \omega t)}$$

$$w = [A_L k_{Lz} \sin(k_{Lz} z) + iA_T k_x \sin(k_{Tz} z)] e^{i(k_x x - \omega t)} \quad (2)$$

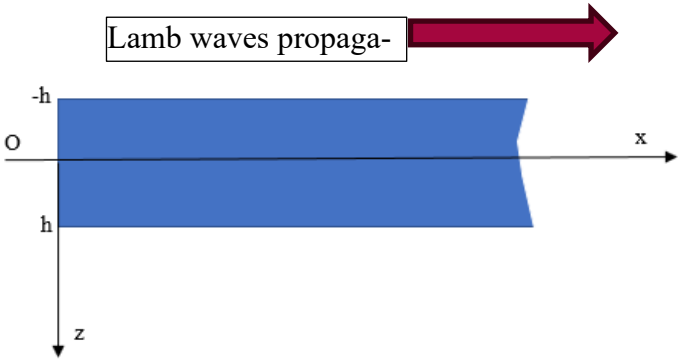

Fig. 2-1 Semi-infinite plate of 2h thickness

The displacements are written based on the scalar and vectorial potential and in their expression several variables and constants may be found, f - frequency, c – velocity of the Lamb wave, c_T and c_L – transversal and longitudinal wave velocities, k_i – wavenumbers, S_T, S_L, A_T and A_L – values of the complex amplitudes.

As for the angular frequency and wavenumbers, the following formulas are considered:

$$\omega = 2\pi f;$$

$$k_x = \frac{\omega}{c}; k_T = \frac{\omega}{c_T}; k_L = \frac{\omega}{c_L};$$

$$k_{Tz} = \sqrt{{k_T}^2 - {k_x}^2}; k_{Lz} = \sqrt{{k_L}^2 - {k_x}^2} \quad (3)$$

Following the expression of displacements (1), (2) for each case and considering elasticity theory (Achenbach 1973), the expressions of dispersion curves may be found as:

Symmetrical:

$$C_s(k_x, \omega) = 4k_x^2 k_{Lz} k_{Tz} \tan(k_{Lz} h) + (2k_x^2 - k_T^2)^2 \tan(k_{Tz} h) = 0; \quad (2)$$

Asymmetrical:

$$C_a(k_x, \omega) = 4k_x^2 k_{Lz} k_{Tz} \tan(k_{Tz} h) + (2k_x^2 - k_T^2)^2 \tan(k_{Lz} h) = 0; \quad (3)$$

Where h is the semi-thickness of the plate (Figure 2.1) and the other terms had been explained above.

Simulations in COMSOL

First results provided by the FEM simulations represent the longitudinal and transversal displacements which are determined in a large range of points, selected both in the middle of the plate and on its surface. These FEM results have been processed in MATLAB as Position-Time plots. The most important results which are obtained in this research are the Position-Time plots of the FEM results for the transversal displacements at the surface (Figure 2.2). Such plots (Griguța and Predoi 2021) indicate the group velocities and modal scattering by the 0.55 mm deep notch in a 3mm thick aluminum plate.

On both plots can be seen the detection of the notch, by the multimodal signal. Important is the first returning echo generated by the notch, proving that this method is adequate.

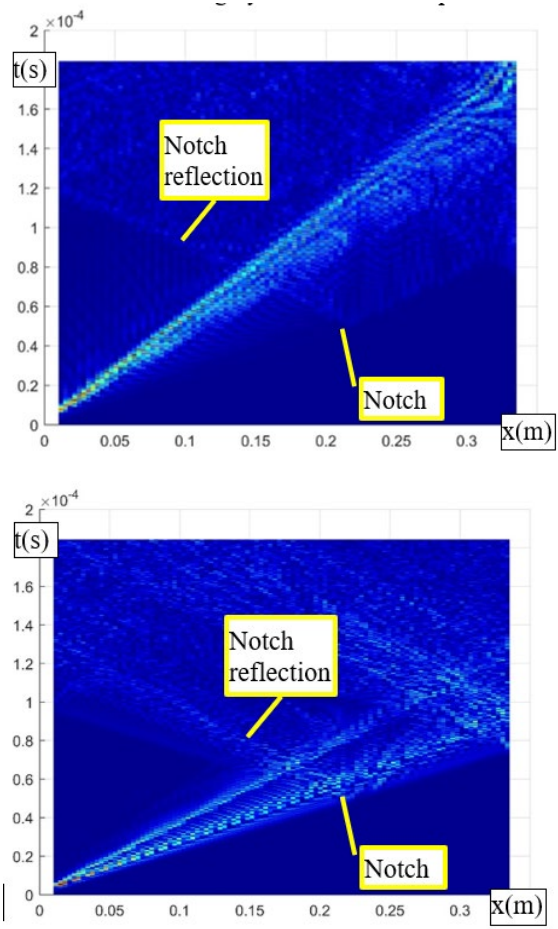

Fig. 2-2 Position-Time plots of the FEM solution for the transversal displacements located on the surface of a plate with a defect for 1 MHz (left) and 2 MHz (right)

Experimental Part

The experimental setup (Fig.2.3) is intended to compare the results extracted from the measurements with the ones from the simulation. Main components in use are a transducer with 1MHz central frequency, pulser-receiver, an oscilloscope, and laser-vibrometer.

Displacements on the surface of the plate were determined using a mobile platform controlled by a stepper motor. The displacements have been measured with the laser vibrometer for positions in the range of 145 mm with the distance between the steps of 0.11mm. There have been considered points of measurements, both before and after the defect positioning as to be comparable to the results from the simulation. All the configurations for pulser-receiver, oscilloscope and vibrometer laser were imposed to optimize the measurements displayed on the oscilloscope.

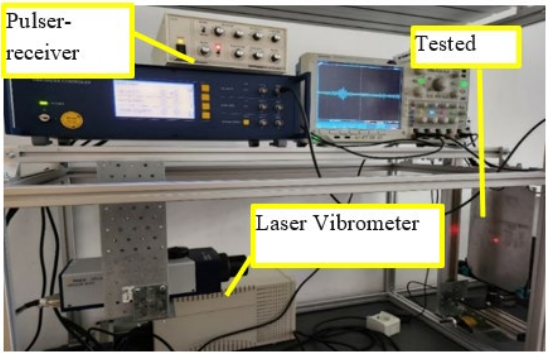

Fig. 2-3 Experimental setup

Results and Discussion

Both simulated results in COMSOL and experimental results have been processed through the same MATLAB code for each set of data, providing the graphical representation of Position-Time plots. Results are presented in Figure 2.4.

The multimodal wave propagation is clearly visible as a set of lines originating at the transducer's position, at the left side of the plot. Having different groups of velocities, it is normal to see the spread of Lamb modes as the time and position increase. Figure 2.4 was marked for easier observation - the thin dotted line, corresponding to the dominant reflected Lamb mode.

Although the position range in the experimental part is different, it can be stated that the graphics present similar slopes for the most prominent mode of propagation, indicating the same group velocities. The defect location is less visible, but the experiment confirms the simulation.

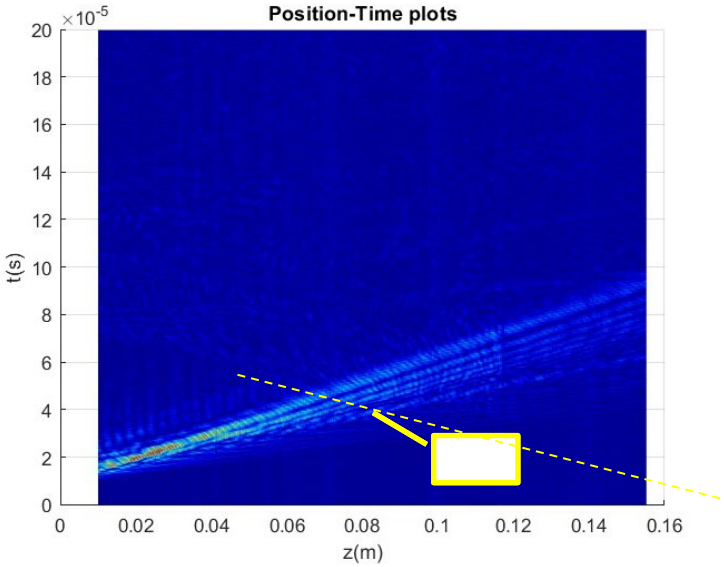

Fig. 2-1 Position-Time plots for 1MHz from experimental measurements

In Figure 2.5 the range of data for the experimental part has been changed to have the same resolution for both graphical representations (experimental and FEM simulation). In order to present the extreme values of errors between the results obtained from experiment and FEM simulation, there have been elaborated a MATLAB code through which the slope of the graph may be read from an image. The results obtained for these errors do not include the possible read errors of pixel positions, since these positions are selected by the mouse pointer on the computer monitor. This is a highly efficient method, being rapid to apply and robust in terms of accuracy especially of the plots have a certain scatter and wobble. In these specific computations, the error for the maximum group velocity is near 0.2% and for the minimum group velocity is near 3.1%.

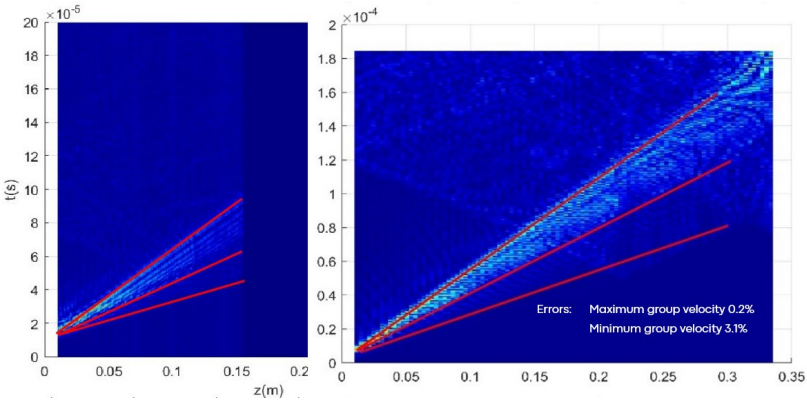

Fig. 2-2 Position-Time plots 1 MHz Experiment Results (left) and FEM simulation results (right). Modal scattering is marked by the red lines.

Conclusions

The use of multimodal Lamb guided waves has been proven to be a useful approach in notch detection. The FEM simulation has provided useful results in predicting the sensitive modes for this purpose. The experimental part is at a preliminary stage. However, the results are encouraging in detecting the presence of a thin notch at a relatively large distance.

It can be emphasized that the detection was done at relatively low frequencies (1 and 2 MHz) which is an important advantage in industrial applications.

As research perspectives are mentioned the determination of the depth of the notch by changing the central frequency of the transducer producing the guided waves. Comparing the amplitudes of the reflected modes for at least two frequencies and based on corresponding FEM simulations, it is expected that the depth of the notch could be deduced.

Moreover, it is known that such asymmetric notch produces a strong dispersion among all the propagating modes, especially at higher frequencies. This dispersion depends on the notch depth and provides another research direction, keeping a single transducer of a fixed central frequency.

References

Achenbach, Jan D. 1973. “Wave Propagation in Elastic Solids”. *North Holland*.

COMSOL AB. 2023. “COMSOL – Software for Multiphysics Simulation”. *COMSOL Multiphysics User Manual*. http://www.comsol.com/.

Graff, Kenneth F. 1975. “Wave Motion in Elastic Solids”. *Dover Publications*.

Griguța, Adrian D.; Predoi, Mihai V. 2021. “Generation of Multi-Modal Lamb Waves for the Inspection of Thin Aeronautical Structures”. *U.P.B. Scientific Bulletin, Series A*, 83(4).

Grondel, Stéphane; Delebarre, Christian; Assaad, Joseph; Dupuis, Jean-Pierre; Reithler, Laurent. 2003. “Fatigue Crack Monitoring of Riveted Aluminium Strap Joints by Lamb Wave Analysis and Acoustic Emission Measurement Technique”. *NDT&E International*, 137–146.

The MathWorks, Inc. 2017. “MATLAB”. https://www.mathworks.com/products/matlab.html. [Accessed 20 November 2017].

Predoi, Mihai V.; Griguța, Adrian D.; Petre, Cristian C. 2022. “Similarities Between Guided and Longitudinal Ultrasonic Waves”. *U.P.B. Scientific Bulletin, Series A*, 84(4).

Predoi, Mihai V.; Petre, Cristian C. 2003. “Contrôle par Ultrasons des Plaques Soudées”. *Ed. Printech*: p. 150.

Predoi, Mihai V.; Rousseau, Michel. 2003. “Recent Results About Lamb Waves Reflection at the Free Edge of an Elastic Layer”. *Acta Acustica*, 89(4).

CHAPTER 3

COMPARISON OF MECHANICAL PERFORMANCE OF MULTI-MODIFIED CEMENTITIOUS MORTARS AND PASTES SENSORS

A.K. THOMOGLOU, M.G. FALARA, F.I. GKOUNTAKOU, A. ELENAS AND C. E. CHALIORIS
DEPARTMENT OF CIVIL ENGINEERING DEMOCRITUS UNIVERSITY OF THRACE, XANTHI, GREECE

Abstract

This comparative analysis focuses on evaluating the mechanical performance of nano-, micro-, and hybrid-reinforced cement mortars and pastes. Specifically, the flexural strength, compressive strength, and flexural toughness of multi-modified cementitious composites strengthened with single-walled carbon nanotubes (SWCNTs), micro-scale carbon fibers (CFs), and their hybrid combination are assessed. The investigation examines the impact of different scales of matrices (mortars and pastes) and varying amounts of nano-modified (0.1, 0.2, and 0.3 wt.% of cement) and micro-modified specimens (0.05, 0.1, and 0.5 wt.% of cement) in conjunction with the collaborative effect of carbon fibers. The comparison of the cement mortars and pastes' mechanical strength and toughness was assessed through 3-point bending and compressive tests on 4 cm × 4 cm × 16 cm and notched 2 cm × 2 cm × 8 cm prisms, respectively. The results reveal that even small quantities of nanotubes and CFs (0.1 wt.% SWCNTs and 0.5% CFs) significantly enhance the mechanical properties and energy absorption of plain cement paste and mortar. Subsequently, this research highlights the strong correlation of

carbon multi-reinforcement of cementitious materials and provides new perceptions for the design of advanced multi-scale structural applications.

Introduction

The excellent mechanical properties of multi-modified cementitious pastes and mortars, attract the interest of researchers worldwide applying them in civil engineering constructions and applications. However, the functionalities of cement-based materials can be enhanced by incorporating carbon nanotubes, graphene, nanoparticles, and chemical additives with sensing abilities to monitor structural health and supplementary factors (Tayeh et al. 2023, e01721; Fantidis et al. 2016, 52–58).

Previous studies have already revealed the beneficial enhancement of the mechanical performance of cement pastes and mortars by incorporating the optimal concentration of nanotubes (SWCNTs or MWCNTs) in the cement matrix (Thomoglou et al. 2023, 2405; Falara et al. 2023, e02066). Additionally, the influence of the different surfactants on carbon fiber dispersion as it turned out played an essential role in the mechanical performance and is still an open field for investigation (Thomoglou et al. 2022, 49; Metaxa et al. 2021, 1430). However, the most impressive results are observed in the case of the synergistic effect of the hybrid incorporation of nano and micro reinforcement. Nevertheless, it is essential to simultaneously investigate the microstructure of the modified composites with non-destructive methods such as X-ray micro-CT (Thomoglou, Fantidis et al. 2023, 4; Fantidis et al. 2016, 52–58; (Kavvadias et al. 2023, 5379).

This research aims to focus on evaluating crucial mechanical properties, such as compressive strength, flexural strength, and flexural toughness of the cement pastes and mortars. A correlation and regression analysis aims to highlight the relations between the mechanical properties of the two different materials, leading to a comprehensive analysis of their interdependencies. On the one hand, correlation analysis is used to assess the relationship between compressive strength, flexural strength, and flexural toughness, by estimating the degree of association between these properties and consequently giving valuable evidence for material characterization. On the other hand, beyond correlation, regression analysis develops mathematical models which predict one variable in connection with the other variables' value (Thomoglou et al. 2023, 2405; Thomoglou, Rousakis et al. 2020, 4411–4425; Thomoglou, Karabini et al. 2023, 53). These models beneficially evaluate the mechanical performance

of cementitious materials in terms of different quantities of incorporated nanotubes, micro-fibers, and hybrid additives.

The results of these analyses will provide valuable tools for material characterization, performance prediction, and structural design in cementitious materials. By conducting this comparative analysis and providing the impact of advantages and limitations of the multi-modified composites, the researchers' community is leading to improve the design regulations for more effective and reliable engineering constructions.

Materials and Methods

In this study, the cementitious materials mortars were cast using a type I standard Portland cement of 42.5 R. To ensure effective dispersion of the carbon nanotubes, nanotube suspensions were prepared in deionized mixing water containing the anionic surfactant sodium dodecyl benzenesulfonate (SDBS). The composition of the SDBS solution is as follows: $C_{12}H_{25}C_6H_4SO_3Na$, which is a colorless salt consisting of various organic compounds. Aldrich and TBP (Tri-n-butyl phosphate) were used to obtain the aqueous/SWCNT/SDBS solutions (Falara et al. 2023, e02066; Thomoglou et al. 2022, 49). The dispersion of SWCNTs is achieved using 60 minutes of ultrasonic energy, while CFs are incorporated through a dry-mix method (Figures 3.1 and 3.2).

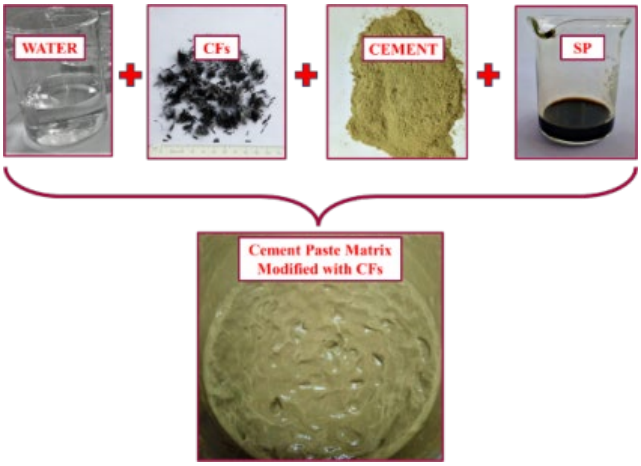

Fig. 3-1 Dry mixing method of CFs incorporation into the cement paste matrix with the included materials

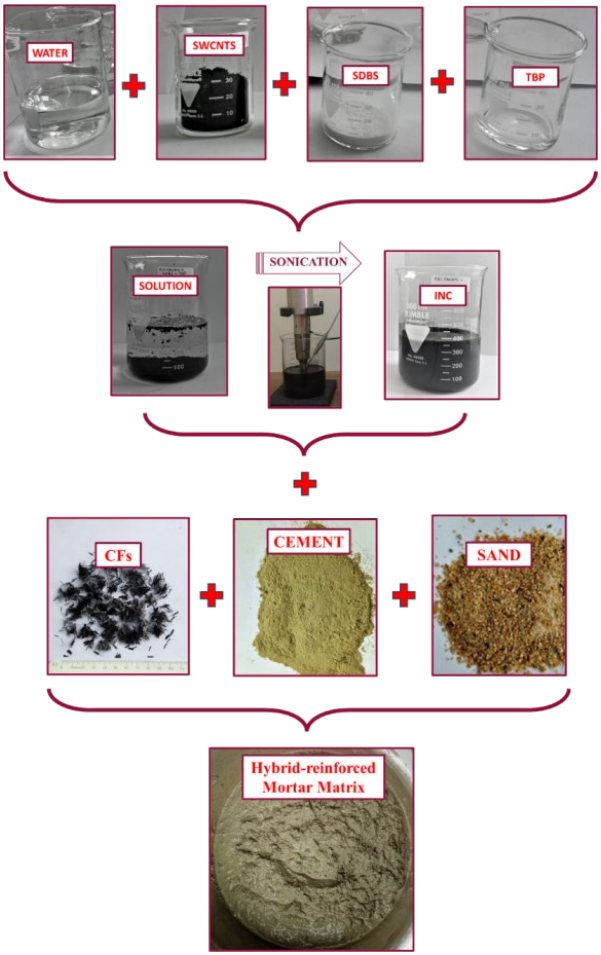

Fig. 3-2 Hybrid reinforcement mixing with micro-fibers (CFs) and nanotubes (SWCNT)

The methodology of this study involved the development of mechanically advanced mortars with nano- and micro-enhancement using SWCNTs and CFs or hybrid, respectively, in varying concentrations. The best combination of nano- and micro-scale enhancements led to the creation of a hybrid mortar with exceptional performance. Mechanical testing techniques were employed to characterize the flexural and compressive strength of the specimens. Three-point bending tests were conducted on 4

cm × 4 cm × 16 cm prisms according to EN 1015–11 standard, and flexural toughness was determined using notched 2 cm x 2 cm x 8 cm prisms based on the Linear Elastic Fracture Mechanics theory (Thomoglou et al. 2023, 2405, Thomoglou et al. 2022, 49, Thomoglou, Fantidis et al. 2023, 4). Compression tests were also performed on the halves of the prisms produced by the bending test. The mechanical testing was carried out using servo-hydraulic and closed-loop testing machines. Overall, this methodology enabled the assessment of the mechanical properties of the multi-modified cement pastes and mortars, providing valuable insights into their performance.

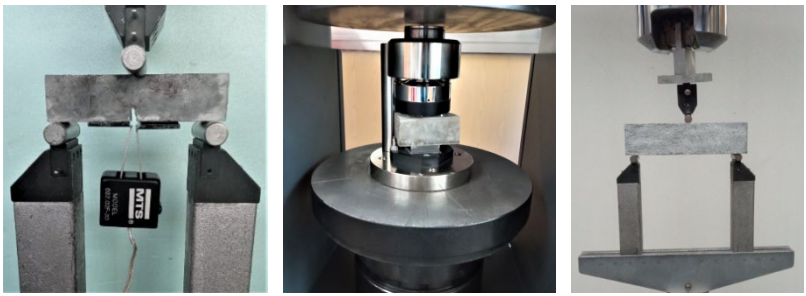

(a) (b) (c)

Fig. 3-3 Experimental test set-up of a) 3-point bending of cementitious composite prisms, b) prism pieces compression, and c) mid-span notched prisms.

Results and Discussion

The statistical analysis shows a strong relationship between the mechanical properties of mortars and cement pastes in terms of nano, micro, and hybrid reinforcement incorporated in the matrix. Correlation and linear regression analysis were performed to determine the best-fit relationship between the measured compressive, flexural strengths, and flexural toughness of the cement pastes and mortars.

The correlation analysis is illustrated in sub-Figures 3.4. (a), (c), and (e). The results expose that the correlation coefficient between variables of flexural strength of the cement pastes and mortars is 0.98, indicating a positive correlation between the strengths (Figure 3.4.a) with the augmentation of nanotube amount. The correlation coefficient between the compressive strength of the two types of cementitious composites demonstrates a good correlation with a coefficient of about 0.90 (Figure 3.4.c) as the SWCNTs amount was improved. This indicates a negative

correlation between these variables. The relationship between the flexural toughness of cement pastes and mortars is depicted in Figure 3.4.e). Specifically, it should be noted that there is a strong correlation with a coefficient r=0.99 as the reinforcement is enhanced (Thomoglou, Fantidis et al. 2023,4).

The regression analysis considered the dependent variables of the mechanical properties with the variation of the reinforcement's concentration. These constants are determined through the regression analysis, along with the regression coefficients (R^2) are presented in Figures 3.4.(b), (d), and (f), illustrating the correlation between the flexural, compressive, and flexural toughness of the two different types of cementitious composites, the cement pastes and the mortars. Upon examining the plots, it is important to highlight that the highest R^2 values were observed in the correlation between flexural strengths of the cement pastes and mortars measured by the SWCNTs augmentation (R^2=0.983). Therefore, flexural strength may be considered a more suitable parameter than compression and flexural toughness for accurate predictions of cementitious composite properties. This finding aligns with previous researchers (Thomoglou, Fantidis et al. 2023, 4).

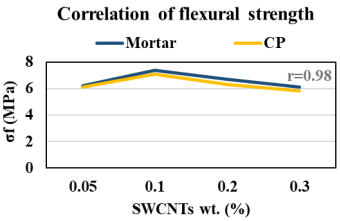

(a)

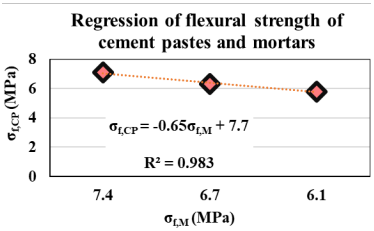

(b)

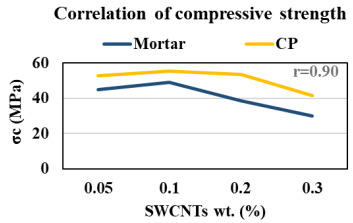

(c)

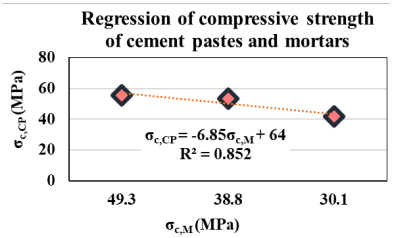

(d)

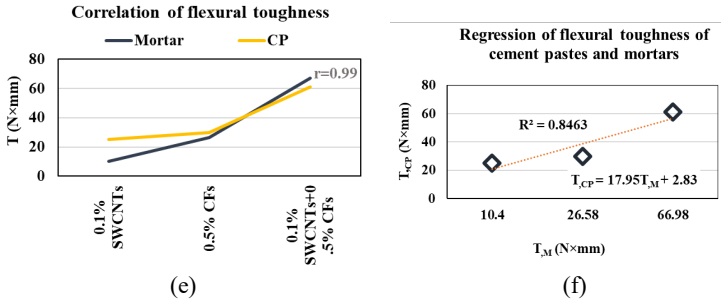

Fig. 3-4 Correlation analysis between (a), (b) flexural strength, (c), (d) compressive strength, and regression analysis of (e), (f) flexural toughness of reinforced cement pastes and mortars with SWCNTs, CFs, and hybrid reinforcement

Conclusions

This study aims to conduct a comparative analysis to explore the correlation between mechanical performance in two different materials: cement pastes and mortars. Specifically, a correlation and regression analysis gains insights into the flexural strength, compression strength, and flexural toughness of the two cementitious materials strengthened with nano, micro, and hybrid reinforcement. The most important results of this research are the following:

- The correlation analysis demonstrated positive relationships between the flexural strength of the cement pastes and mortars with the simultaneous augmentation of the nanotube amount. The correlation coefficient between these variables was found to be 0.98.
- The compressive strength of the cementitious composites showed a negative correlation with the concentration augmentation of SWCNTs and a correlation coefficient of about 0.90.
- The flexural toughness of cement pastes and mortars exhibited the strongest correlation with a coefficient of 0.99 as the reinforcement was enhanced.
- The highest regression coefficient R^2=0.983 value was presented in the correlation among flexural strengths of cement pastes and mortars, particularly with the SWCNTs concentration increase.
- Results reveal that flexural strength is a more reliable factor compared to compression and flexural toughness when predicting the properties of cementitious composites.